

Combustion Mechanism of the Multiway Impinging-type Burners

Jing-Tang Yang,* Han-Chang Cheng, Fu-Ane Chen, and Shiang-Fu Chen
Department of Power Mechanical Engineering, National Tsing Hua University
Hsinchu, Taiwan 30043

E-mail: jtyang@pme.nthu.edu.tw; Fax: 886-3-5724242

* Professor, the corresponding author

Extended Abstract

1. Introduction:

The geometric configuration of a burner impinges on the transport features of the unburned gases in pre-heat stage, and, thus on the flame structure of the combustion system. Therefore, the design of the geometry and the mixing mode between the fuel and the air are crucial to the combustion performance of the burner. Hou *et al.* (1991) conducted experiments in counter-impinging flame, concluding that premixed flame had more intensive combustion reactivity than those of premixed flame and diffusional flame. Yang *et al.* (1997) and Yang and Yen (1996) reported that by manipulating the double concentric jets of a disc bluffbody, the flame modes were altered drastically. Dismile *et al.* (1995) observed the jet flames impinging to each other at an inclined angle and reported that the mixing effect was significantly improved. The method of inclined injection was also often utilized inside the side-dump combustors (Laredo *et al.*; 1991, Liou *et al.*, 1998). All cases imply that there are plenty ways through improving flow patterns to intensify the combustion behavior of burners. Yang and Kao (1999) proposed the impinging design within a dip and built them inside the exit of the high-loading burner and reported that the overall performance was significantly enhanced. The related flame structures and combustion mechanisms still need in-depth exploration.

2. Experimental Design:

Three types of the burners, a two-way impinging burner, a three-way impinging burner and a flat-type burner, as shown in Fig. 1, were systematically studied. The width of the burner was 12 mm and the depth of the dip was 6 mm. The major controlling parameters were the flow rates of the fuel and the primary air. The schematic diagram of the experimental setup is depicted in Fig. 2. The fuel was the commercial-grade propane gas (95% C₃H₈, 3.5% C₂H₆, and 1.5% C₄H₁₀). The burner was placed in a still-air environment and protected with a fine-wire mesh screen from any outside turbulence perturbation. Main theme of the experiment was on the comparison among the three burners, especially on the flame patterns, the stable operation diagram, the distributions of velocity and temperature in the flow, the thermal and flow characteristics within the dips of the impinging burners.

Flame configurations were observed and recorded with a Sony V505 digital camera and a V-8 video camera. The combustion performance diagram for each burner was determined by systematically adjusting the flow rates of the fuel and the primary air, respectively. Mean flow temperature and temperature fluctuation were measured by an R-type thermocouple with diameter 25 μm . In each measurement point, 100 temperature data were taken with the period of 0.3 second. To eliminate the error of the response delay of the sensor, only the last 60 points were taken to do the statistical analysis. The velocity data were measured with the TSI two-component laser-Doppler velocimetry and the related information can be referred to Chen *et al.* (1997).

3. Results and Discussion

The mode and color of the flame for each burner altered with the variation of the air-fuel ratio. Figure 3 shows five typical flame configurations corresponding to the equivalence ratios (f) of 0, 0.4, 0.6, 0.9, 1.3, respectively, and the corresponding combustion-regime diagrams are depicted on Figs. 4 to 6. The flames modes of $f = 0.4$ (yellow-tip flame), $f = 0.6$ (central-green flame) and $f = 0.9$ (blue flame) were further analyzed quantitatively. Since both two-way and three-way impinging burners have the steric structure, both of them released much energy per unit volume. From the contrast of

the three combustion-regime diagrams, the two impinging burners generated much broadened range for stable operation, especially for the higher loading of the fuel, as compared with that of the flat-type burner. Since the impinging burners induced a higher flame propagation speed within the dip of the exit, the two-way impinging burner encountered the flash back problem at the fuel flow rate of 0.5 liter/min and the central-green flame ($f = 0.6$) range was relatively narrow. The design of the additional central jet flow in the three-way impinging burner could prevent the flash back at stoichiometric combustion, but it might moderate the combustion activity during very rich burning. The contrast of the flames in Fig. 7 illustrate that at $f = 0.9$ the flame cones for the two impinging-burners were stably sustained within the dips of each burner. The three-way burner had one extra flame staying on the bottom of the dip, which altered the combustion performance significantly. General speaking, the stable operation range of each flame mode for the three-way burner was superior to that of the two-way impinging burner.

The flow temperature distributions downstream the burner exits are shown in Figs. 8 to 10, respectively. The temperature distributions in Fig. 8 indicate that the behavior of the flat-type burner was similar to that of the traditional jet burner and the high-temperature zone was always located around the shear layers of the jet. The flame height at $f = 0.6$ was around 7 times of the flat-type burner width whereas that of the impinging burners was less than 5 times. The thermal behavior of the impinging burners at higher fuel rates was quite different from that of the flat-type burner. Because the impingement of the inclined jets, the vertical flow velocity around the ignition zone was significantly reduced and the low-velocity zone was enlarged. Both effect resulted in intensive preheat and reaction near the exit of the impinging-type burners, and, the entire flame thus became narrower and shorter. Instead of the cold core in the flat-type burner, high temperature core ($T > 1100^\circ\text{C}$ for $f > 0.5$) developed and extended from the exit to $y/w = 5$ for both impinging burners, as shown in Figs. 11b-c and 12b-c. Since the blue flame cones were generated and resided within the dip, the flow temperature was higher than 1500°C near the exit of the burner. Due to the distinct impinging patterns among the three jets, the three-way impinging burner had a dislike flame structure within the dip and resulted in a broader cold core at $f = 0.4$ whereas a narrower flame zone for $f > 0.5$.

The temperature distributions in the dip of the impinging burners were further investigated and the partial results are depicted in Figs. 11 and 12. At $f = 0.6$ the flow temperature within the dip already exceeded 700°C and that on the two sides of the exit even exceeded 1100°C . When the equivalence ratio was 0.9, the flow temperature within the entire dip was over 1200°C except in the vicinity of the injection slots and the flow heated up to 1500°C before leaving the exit. Besides, the flame of the two-way impinging burner was located in the middle part of the dip whereas that of the three-way impinging burner contained a higher and broader region of high-temperature and flame very close to the bottom. The distributions of the temperature fluctuation within the dip further confirm that both thermal and flow features of the two impinging burners were apparently different. The velocity distributions along the line of $x/w = 0$ of two impinging burners operating respectively at $f = 0.4, 0.6$ and 0.9 are shown in Fig. 13. Due to the additional central jet flow and the impingement from two sides, velocities of three-way impinging burner were faster in the bottom and much slower downstream than those of two-way impinging burner. As y/w was greater than 0.1, the flow velocities along the line of $x/w = 0.1$ for both impinging burners were almost equivalent and insensitive to f . The horizontal velocity distributions along the line of $x/w = 0.1$ of two impinging burners at $f = 0.4, 0.6$ and 0.9 , respectively, are shown in Fig. 14. Due to the effects of mutual impingement, the horizontal velocity magnitudes were negative between $y/w = -0.2$ and 0.4 as f was 0.4. At $f = 0.6$, the impingement effect of three-way impinging burner extended to $y/w = 0.6$ because of the central jet flow. At $f = 0.9$, the fuel flow rate was greater, thus the velocity and the impinging momentum was greater. The region of negative horizontal velocity extended to $y/w = 0.7$ or even more downstream.

4. Conclusions

The flame structure of multi-way impinging-burners were experimentally investigated and

systematically compared with those of the flat-type design. Instead of the traditional 2-D layout, the 3-D concept and the impinging flow design within the dip of the burner were adopted for both the two-way and three-way impinging burners. The experimental results of flame and temperature measurements indicated that the new designs effectively reduced the flow velocity and restructured the flow pattern. It also generated small recirculating bubbles within the dip and significantly preheated the air/fuel mixture. All these factors raised the temperature of the combustion products, enlarged the stably operating range, and improved the combustion instability of the burners. Similarities and differences in reacting flow between the two-way and the three-way impinging burners were also discussed in detail. Quantitative studies on mean flow structure, mean temperature distribution, and flow fluctuations further confirmed the superior combustion mechanism of these impinging-burners.

5. Acknowledgement

This work was supported by the National Science Council of the Republic of China (Taiwan) under grants NSC-90-2212-E-007-073. We thank Dr. Chang, Chia-Chih and Mr. Kao, Chih-Yong for the inspiring discussion and the assistance of the experimental work.

6. References

- Hou, S.S., Chang, C.K., and Lin, T.H., 1991, "An Experimental Investigation on Multiflame Burning Structure in Conserved System," *Combustion Science and Technology*, **79**, 35.
- Yang, J. T., Chang, C. C., and Lee, Y. P., 1997, "Thermal Analysis of Non-premixed Flame Behind a Disc-Type Stabilizer with a Central Fuel Jet," *Proceedings of the 16th International Colloquium on the Dynamics of Explosion and Reactive Systems*, Cracow, Poland, August 3-8, p. 117.
- Yang, J. T. and Yen, C. W., 1996, "Reacting Flow over a Non-Traditional Flame Stabilizer," *Combustion Science and Technology*, **112**, 95.
- Disimile, P.J., Savory, E., and Toy, N., 1995, "Mixing Characteristic of Twin Impinging Circular Jets," *Journal of Propulsion and Power*, **11**, 1118.
- Laredo, D., Levy, Y., and Timnat, Y. M., 1991, "Study of Two-phase Flow for a Ramjet Combustor," *J. Propulsion and Power*, **7**, 724.
- T.M. Liou, Y.Y. Wu and H.L. Lee, July 1998, "Visualization of Impingement Flows in a Chamber With Multiple Inlets," *Int. J. Flow Visualization and Image Processing*, **5**, 225.
- Yang, J. T. and Kao, C. Y., 1999, "Convective Impinging-Type High-Loading Burner," ROC (Taiwan) Patent No. 149086.
- Chen, Y. C., Chang, C. C., Pan, K. L., and Yang, J. T., 1998, "Flame Lift-off and Stability Mechanisms of Nonpremixed Jet Flames in a Bluff-body Burner," *Combustion and Flame*, **115**, 51.

List of Figures

Fig. 1 Photographs of three types of the burners.

Fig. 2 Schematic diagram of the experimental apparatus.

Fig. 3 Photographs of flame structures of the two-way impinging burner, fuel volume flowrate = 1.0 L/min.

Fig. 4 Stable operation diagram of the flat-type burner.

Fig. 5 Stable operation diagram of the two-way impinging burner.

Fig. 6 Stable operation diagram of the three-way impinging burner.

Fig. 7 Photographs of the blue flame of two impinging-burners, fuel volume flowrate = 1.0 L/min.

Fig. 8 Distributions of mean temperature of the flat-type burner, fuel volume flowrate = 1.0 L/min.

Fig. 9 Distributions of mean temperature of the two-way impinging burner, fuel volume flowrate = 1.0 L/min.

Fig. 10 Distributions of mean temperature of the three-way impinging burner, fuel volume flowrate = 1.0 L/min.

Fig. 11 Distribution of mean temperature within the dip of the two-way impinging burner.

Fig. 12 Distribution of mean temperature within the dip of the three-way impinging burner.

Fig. 13 Distributions of velocity of the impinging burners ($x/w = 0$), $\phi = 0.4, 0.6$ and 0.9 .

Fig. 14 Distributions of horizontal velocity of the impinging burners ($x/w = 0.1$), $\phi = 0.4, 0.6$ and 0.9 .

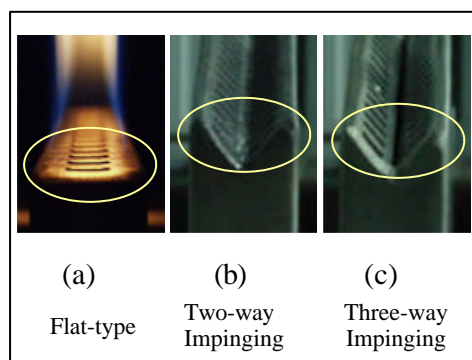


Fig. 1

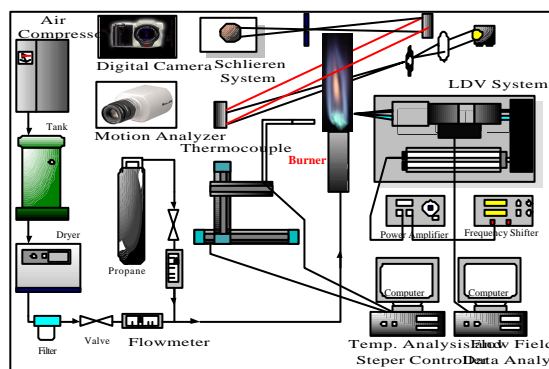


Fig. 2

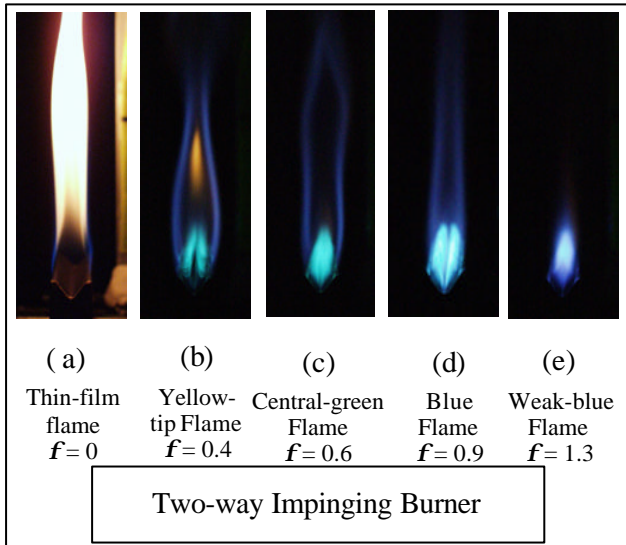


Fig. 3

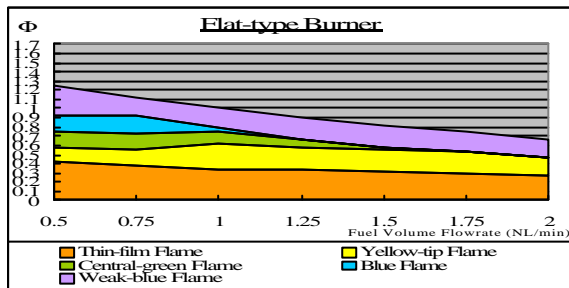


Fig. 4

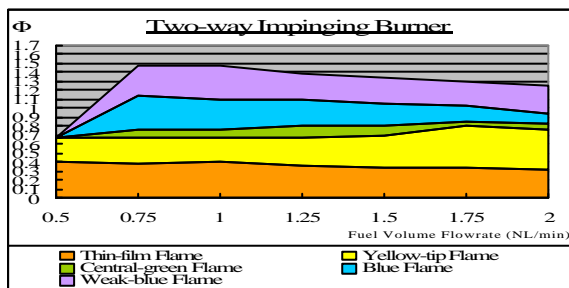


Fig. 5

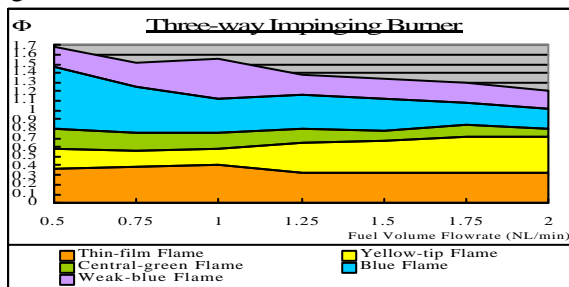


Fig. 6

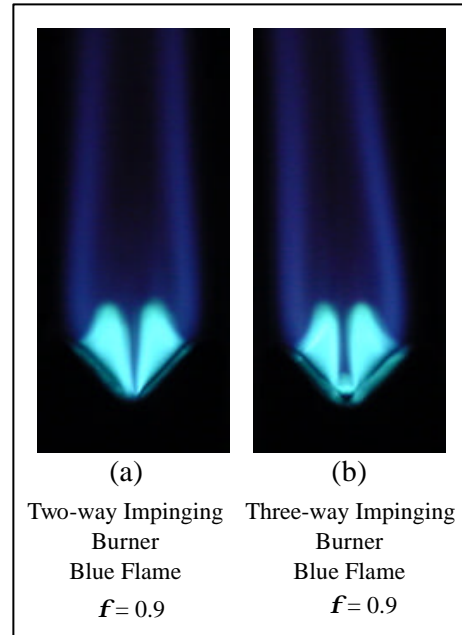


Fig. 7

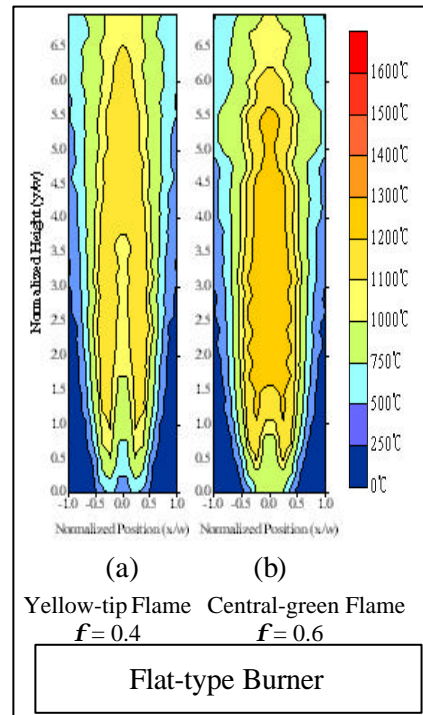


Fig. 8

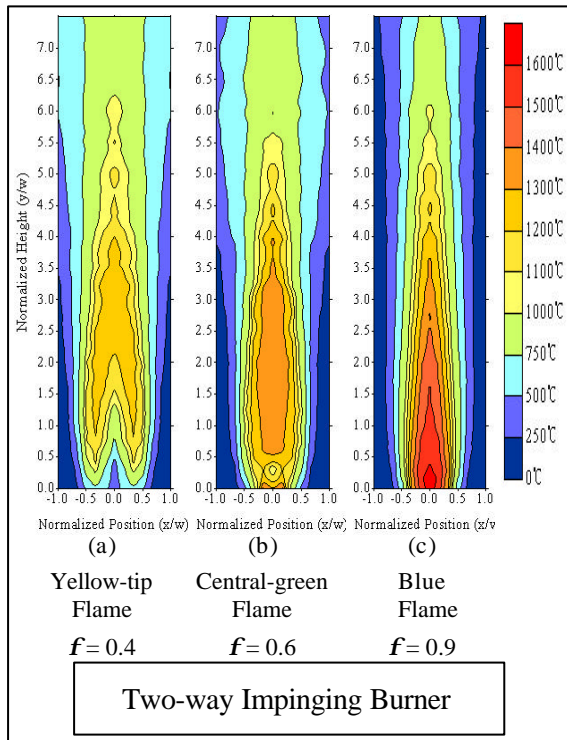


Fig. 9

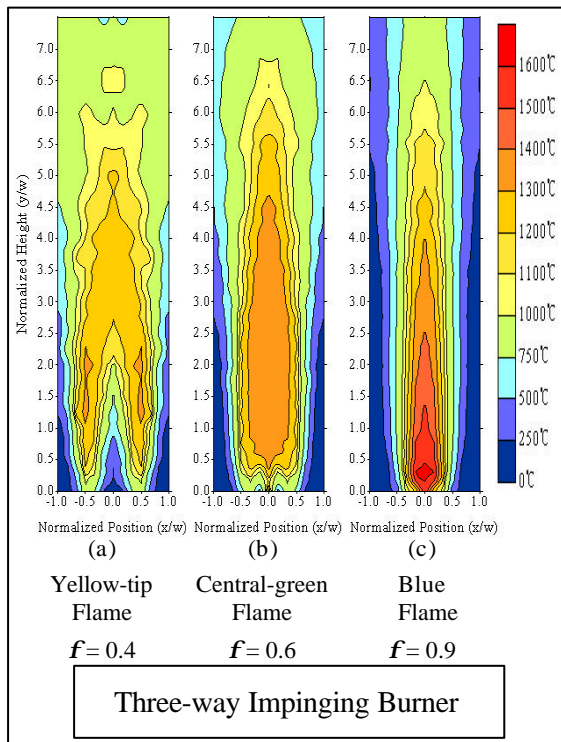


Fig. 10

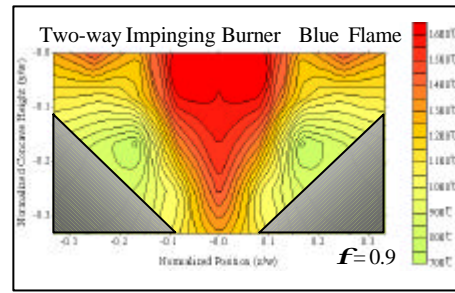


Fig. 11

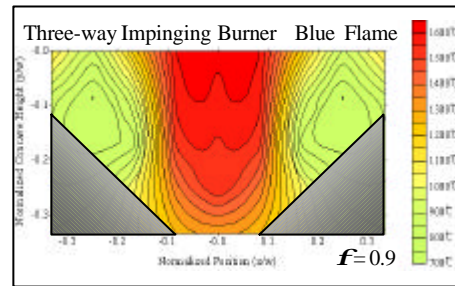


Fig. 12

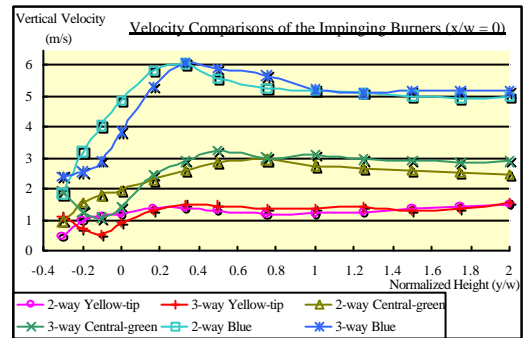


Fig. 13

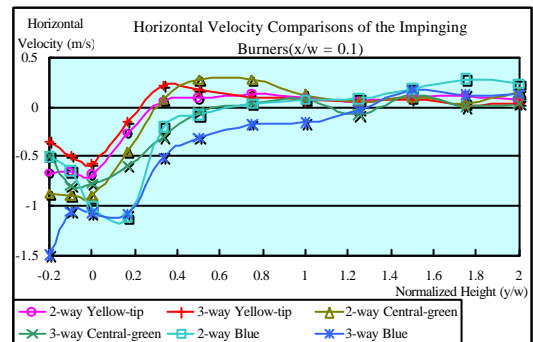


Fig. 14